Nuclear Instruments and Methods in Physics Research A 660 (2011) 15–21

Contents lists available at SciVerse ScienceDirect

Nuclear Instruments and Methods in Physics Research A

journal homepage: www.elsevier.com/locate/nima

Wiggler improvement based on single axis magnetic measurement, synthesized 3-D field simulation of trajectories and sorting of lateral focusing magnets

H.S. Marks [a,*], M. Volshonok [a], E. Dyunin [a], A. Gover [a], Y. Lasser [b], R. Shershevski [b], A. Yahalom [b]

[a] Department of Physical Electronics, Faculty of Engineering, Tel Aviv University, IL-69978 Tel Aviv, Israel
[b] Department of Electrical and Electronic Engineering, Ariel University Center of Samaria, Ariel, Israel

ARTICLE INFO

Article history:
Received 23 August 2011
Accepted 6 September 2011
Available online 17 September 2011

Keywords:
Wiggler
Undulator
Optimization
Magnet Sorting

ABSTRACT

A method is presented for correcting magnetic field imperfections in an assembled wiggler of the Halbach configuration. The method is employed in a configuration in which lateral focusing is needed along the wiggler (at low beam energies and large length) and is provided by external magnet bars alongside the wiggler. Field deviations in both vertical and lateral dimensions due to wiggler imperfections are repaired by sorting and reassembly of the focusing magnets. A single Hall probe measurement along the wiggler axis and individual measurements of the focusing magnet bars provide sufficient data for sorting and optimal choice of the positions of the focusing magnets. Moreover, this data enables 3D simulation of the e-beam transport trajectories in the virtually synthesized field of the wiggler with the contemplated repair configuration of the focusing magnet bars before actually assembling them. It thus provides in advance a realistic prediction of the quality of the repair.

1. Introduction

Free electron lasers are devices that transform the kinetic energy of electrons into electromagnetic radiation as they pass through a periodic magnetic structure, called a wiggler or undulator. They can operate with a wide range of frequencies, exhibiting high power, high efficiency, and tunability [1].

The key element in any FEL is the wiggler. It generates a nearly sinusoidal transverse magnetic field on axis, which provides the wiggling motion of the electron beam, and also keeps it focused and confined to the axis. Imperfections in this magnetic field may compromise the operation of the FEL [15], and may prevent good transport of the beam through the apertures of the wiggler. In most cases wigglers are made of permanent magnets. A popular wiggler design scheme is a linearly polarized wiggler in the Halbach configuration [2]. In addition to providing a nearly sinusoidal transverse vertical magnetic field on axis, which generates electron wiggling in the lateral (x) dimension, the Halbach wiggler provides a natural focusing effect (betatron oscillation motion) in the vertical (y) dimension. To compensate for lack of focusing (and even small defocusing effects) in the lateral dimension, quadrupoles are usually used to converge the beam before injection into the wiggler. However, at low beam energies and for long wigglers, additional focusing is required along the wiggler in order to limit the lateral expansion of the beam. This can be produced by pole face canting, parabolic pole face shaping, or in the case of the simple Halbach configuration, by adding quads to the structure either encompassing the wiggler or in spaces between properly terminated short wiggler sections.

A compact and simple solution for lateral focusing along a Halbach wiggler that is especially fitting for low energy beam transport is shown in Fig. 1. The focusing is provided by a linear array of bar magnets placed with a small spacing between them along the length of the wiggler on both of its sides and polarized in opposite vertical dimensions. Such a configuration was successfully employed in the Israeli electrostatic accelerator free electron laser (EA-FEL) [3]. The experimental employment of the wiggler improvement scheme described in this article was carried out on this structure.

Various schemes have been proposed for the optimization of wigglers with permanent magnets [4–8]. The optimizations are typically required due to imperfect alignment of the polarization fields of the magnets together with differences in field strengths between magnets. However, for an existing wiggler these optimization methods require the disassembly of the main body of magnets. Other methods have been developed based on placement of iron shims to correct field errors without disassembly [9]. Another suggested method avoiding disassembly requires having the ability to adjust individually the distance of lateral focussing magnets from the central wiggler axis [10].

* Corresponding author. Tel.: +972 3640 5410.
E-mail addresses: harry@eng.tau.ac.il, harry_s_marks@hotmail.com (H.S. Marks).

0168-9002/$ - see front matter © 2011 Elsevier B.V. All rights reserved.
doi:10.1016/j.nima.2011.09.004

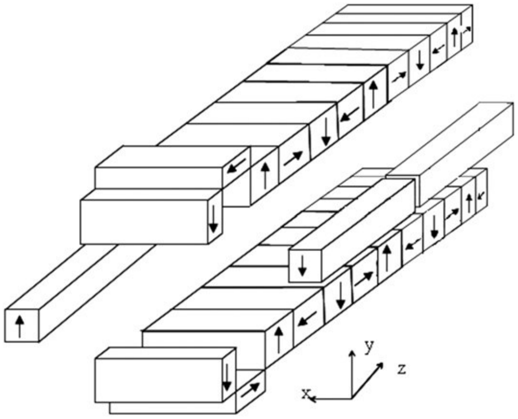

Fig. 1. Diagram showing the relative positions of the principal and lateral magnets within the wiggler.

In all these previously conceived methods the repair quality is judged only from measurement of the magnetic field along the axis. This is a highly inaccurate way to predict the e-beam trajectories, especially when the beam is focused along the wiggler. In such a case, an elaborate, costly, and time consuming 3-D mapping of the wiggler field is needed in order to predict reliably the beam trajectories and the quality of the repair. The advantage of the method proposed in this article is that it enables the construction of a virtual 3-D field based on a single scan of the field and have better prediction of the quality of the repair in advance. The successful use of the method is demonstrated by its employment on the compact focusing wiggler configuration of Fig. 1, but it can be extended to any other kind of permanent magnet planar wiggler with nearly unity susceptibility, if sufficient adjustable external focusing elements are available along the wiggler with individually known magnetic field maps.

The lateral focusing wiggler configuration shown in Fig. 1, is an exceptionally compact way to provide external focusing, and is a good solution for confining the expansion of a low energy beam in a relatively long wiggler. But, this configuration is also a good example for demonstrating the correction method based on external field that is proposed here. The externally mounted bar magnet lateral focusing scheme provides the advantage of wiggler field imperfection repair by easy disassembly and sorting of the focusing magnet bars. This method avoids the laborious task of re-ordering all the principal magnets, and enables wiggler field correction by using an algorithm that selects optimum pairs of only the lateral focussing magnets. It also avoids the need to fully map the magnetic field inside the wiggler in order to assess the quality of the repair. A single Hall probe field measurement along the axis provides the data on the imperfection of the wiggler field. As the 3-D magnetic field of rectangular bar magnets can be easily modelled [13], and because for magnetic materials like SmCo the superposition of the magnet fields is an acceptable approximation, the wiggler field measurement data and the separately measured data of the individual focusing-magnets are sufficient for employing a focussing magnet pairing algorithm. Moreover, it enables 3D beam transport simulations based on a virtually synthesized field of the measured magnets in the contemplated pairing configuration. The simulation makes it possible to examine the improvement in the beam trajectories before actually reassembling the focussing magnet pairs. This method has an advantage over techniques of shimming or individual repositioning and adjustment of the focusing magnets, which are more elaborate, and require readjustment processes on the basis of re-measurement and comparison of magnetic field measurements. They also do not enable testing the quality of repair by 3D simulations unless very detailed 3D field mapping is carried out at each adjustment step.

1.1. Transport in a planar wiggler with lateral focussing

The magnetic field of an ideal planar wiggler (laterally infinite) can be modelled with the following equations [11]:

$$B_y^W(y,z) = B_0^W \cos(k_w z)\cosh(k_w y) \tag{1}$$

$$B_z^W(y,z) = -B_0^W \sin(k_w z)\sinh(k_w y) \tag{2}$$

where B_0^W is the amplitude of the magnetic field due to the wiggler, and k_w is the wave number of the magnetic structure. The condition $\vec{\nabla} \times \vec{B} = 0$ entails the existence of a magnetic potential Φ_M such that $\vec{B} = -\vec{\nabla}\Phi_M$. Moreover, since $\vec{\nabla} \cdot \vec{B} = 0$ the magnetic potential satisfies the Laplace equation $\vec{\nabla}^2 \Phi_M = 0$. It can be easily seen that $\Phi_M = -(B_0^W/k_w)\cos(k_w z)\sinh(k_w y)$ satisfies the Laplace equation and entails the magnetic field component Equations. (1) and (2).

The electron trajectory in a static magnetic field satisfies the force equation

$$m\gamma \frac{d^2\vec{r}}{dt^2} = -e\vec{v} \times \vec{B} \tag{3}$$

where $-e$ and m are the electron charge and rest mass, respectively t is time, and $\vec{r}$ and $\vec{v}$ denote the electron location and velocity. The relativistic Lorentz factor γ is given by $\gamma = [1-(v/c)^2]^{-1/2}$, in which c is the velocity of light in vacuum. Assuming that the z component of velocity is high with respect to all other velocity components and has the average value v_{0z} (and so $v_z \gg v_y$), one can re-parameterize the electron trajectory in terms of the independent variable z such that: $dz = v_{0z}\, dt$;

$$m\gamma \frac{d^2\vec{r}}{dz^2} \cong \frac{e}{v_{0z}^2}(v_{0z}B_y^W\hat{x} + v_x B_z^W\hat{y} - v_x B_y^W\hat{z}) \tag{4}$$

Hence, for any initial velocity in the x direction (v_{0x}) and initial displacement in the x direction (x_0) the x component has a solution of the form [12]

$$x = \frac{-eB_0^W}{v_{0z}m\gamma k_W^2}\cosh(k_w y)\cos(k_w z) + \frac{v_{0x}}{v_z}z + x_0 \tag{5}$$

Averaging over the wiggler periodicity, the centroid trajectory is:

$$\bar{x} = \frac{v_{0x}}{v_z}z + x_0 \tag{6}$$

Similarly we can calculate the y displacement in the limit $k_w y \ll 1$:

$$\bar{y} = y_0\cos(k_\beta z) + \frac{v_{y0}}{v_{0z}k_\beta}\sin(k_\beta z) \tag{7}$$

Here we define the betatron wave number $k_\beta = eB_0^W/\sqrt{2}v_{0z}m\gamma$

In which we assume that $k_w y \ll 1$.

Clearly the wiggler field provides a focussing force in the vertical (y) dimension, which confines the electron trajectories within the limit $|y(z)| < [y_0^2 + (y_0'/k_\beta)^2]^{1/2}$ (since $y_0' = (v_{0y}/v_{0z})k_\beta$). In the lateral ($x$) dimension, the electron wiggles with period $\lambda_W = 2\pi/k_w$, but at the same time it drifts aside if v_{0x} is non-zero.

In order to provide lateral focussing one can superimpose a quadrupole field on the wiggler as shown in Fig. 1 using bar magnets placed along the wiggler on both its sides polarized vertically in opposite ways, so that their net field on axis cancels out, but they produce near the axis a linear gradient field that has a magnetic potential $\Phi_M^F = -\alpha_R xy$ near the axis, such that:

$$B_y^F = -\alpha_R x \tag{8}$$

$$B_x^F = -\alpha_R y \tag{9}$$

$$\alpha_R = -\frac{\partial B_y^F}{\partial x} = -\frac{\partial B_x^F}{\partial y} \text{ at } x=0, y=0 \tag{10}$$

Such a quadrupole field provides focussing in the lateral dimension. However, it inevitably contributes a defocusing field in the vertical dimension, thus reducing the vertical focussing effect provided by the wiggler. Depending on the beam emittance values in the x and y dimensions ε_x, ε_y and the physical aperture dimensions for e-beam propagation inside the wiggler, there is an optimal value of α_R for the best confinement of electrons near the axis within the wiggler acceptance aperture.

Solving for the electrons trajectories in the combined field (1), (2), (8), and (9), one finds instead of Eqs. (3)–(7) that the x-wiggling motion is superimposed on betatron oscillation motion of wave number k_{bx} in the x direction ($\bar{x}(z)$), and the betatron oscillation motion in the y direction ($\bar{y}(z)$) has a reduced wave number k_{by}:

$$x(z) = \bar{x}(z)\text{-}x_W \cosh(k_W y)\cos(k_W z) \tag{11}$$

$$\bar{x}(z) = (x_0 + x_W \cosh(k_W y))\cos(k_{\beta x} z) + \frac{\upsilon_{x0}}{\upsilon_{z0} k_{\beta x}} \sin(k_{\beta x} z) \tag{12}$$

$$\bar{y}(z) = y_0 \cos(k_{\beta y} z) + (\upsilon_{y0}/\upsilon_{z0} k_{\beta y})\sin(k_{\beta y} z) \tag{13}$$

$$k_{\beta x} = \sqrt{\frac{e\alpha_R}{\gamma m \upsilon_{0z}}} \tag{14}$$

$$k_{\beta y}^2 = \frac{k_\beta^2}{1-(k_{\beta x}/k_w)^2} - k_{\beta x}^2 \tag{15}$$

$$x_W = \sqrt{2}\frac{k_\beta}{k_W^2 - k_{\beta x}^2} \tag{16}$$

When considering a beam of finite emittance values $\varepsilon_x = \pi x_{b0} x'_{b0}$ and $\varepsilon_y = \pi y_{b0} y'_{b0}$, where x_{b0}, y_{b0}, and x'_{b0}, y'_{b0} are the beam radii and half angular spread values at the beam waist, repectively it is optimal to inject the beam into the wiggler entrance at its waist and focus it so that its waist dimensions at the entrance are [11]

$$x_{b0}^{opt} = k_{\beta x0}^{-1} x'^{opt}_{b0} = (\varepsilon_x/\pi k_{\beta x})^{1/2} \tag{17}$$

$$y_{b0}^{opt} = k_{\beta y0}^{-1} y'^{opt}_{b0} = (\varepsilon_y/\pi k_{\beta y})^{1/2} \tag{18}$$

Under these conditions the beam propagates along the wiggler without scalloping. This is the condition for minimum excursion of beam electron trajectories away from the axis. Furthermore it is the condition for minimum axial velocity spread (a desirable condition for FEL operation).

The wiggler that is the subject of this work is composed of SmCo bar magnets. Its length L_W is 1.201 m, and it is comprised of an entrance section to place the electrons in correct on-axis trajectories, 26 magnetic periods of length 44.4 mm, and an exit section, so that the electrons leave the wiggler along the central axis. The periods are arranged in a Halbach planar configuration [2].

For lateral focussing, 23 magnets of length 50.8 mm, similar to the magnets that form the main wiggler field, were placed along the length of the wiggler on either side. Gaps between these magnets were filled with Teflon spacers of thickness ~1.4 mm.

2. Method of repair

The magnetic fields of the wiggler in the transverse x–y directions were measured along 5-axes using a Hall Probe (F.W. Bell 9950 YOB-25) These axes were at $x=y=0$ mm from the centre of the wiggler's mechanical/geometrical axis, $x=\pm 4$, $y=0$ mm, and $x=0$, $y=\pm 4$ mm. The probe was moved forward in steps of 1 mm using a stepper motor. At each step a reading was taken and recorded using a data acquisition card and Labview software. The average peak amplitude of the principal field along the central axis was 1.93 kG. It was determined from this data and from direct calliper measurements of the assembled magnets in the wiggler that the short range and long range periodicity $\lambda_w=44.4$ mm of the magnetic field along the entire length, determined by the dimensions of the magnet bars (11.1 mm each), was accurate to within ± 0.1 mm. However, the periodic wiggler field was seen to be superimposed over a slowly varying (relative to the wiggling period) magnetic field variation, which originates from variation in the strength and orientation of the magnet bars magnetizations of either the wiggler or focusing magnets.

Once these first measurements had been made the lateral focussing magnets were removed. Fig. 2 shows the measurement of $B_x(z)$ along the axis before disassembly of the focusing magnets. This field ideally should be null. The periodic modulation component of 30 G amplitude on top of the random field variation retains a constant phase, and therefore should be attributed to orientation inaccuracy of the Hall probe (misalignment of less than 1^0 –less than the positioning accuracy of the probe–would pick up such a component of the strong 1930 G amplitude B_y field). This parasitically picked-up periodic magnetic field component is superimposed over a slowly varying random magnetic field of up to 50 G (shown in Fig. 2 after filtering out the periodic component of the measured field). This random field pattern is mainly a result of imperfect alignment in the y direction of the magnetization in either the wiggler or the focusing magnets. This random slowly varying B_x component was considered to be the main cause for electron trajectory deviation from the ideal y-dimension betatron oscillation pattern (7), and the purpose of the wiggler repair procedure was to reduce the effect of this random field by re-sorting *only* the focusing magnets and reassembling them to minimize this random field component. Similarly, filtering of the $B_y(z)$ measured data revealed a slowly varying randomly fluctuating $B_y(z)$ magnetic field of up to 30 G amplitude superimposed on the periodic $B_y(z)$ field component of high amplitude 1930 G.

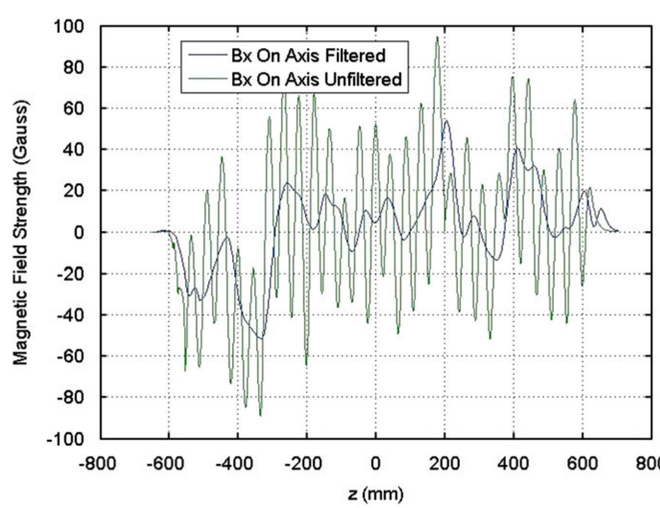

Fig. 2. Measured B_x field and its random perturbation component obtained by filtering out the coherent periodic component.

In addition to repair of the $B_x(z)$ fluctuations, the sorting and reassembling process of the focusing magnets was also aimed to minimize these random B_y fluctuations, which originate mainly from variations in the magnetization strengths of the magnet bars, and are responsible for an averaged deviation in the electron trajectories from the ideal x-dimension betatron oscillation pattern (12).

The periodic component in the measured $B_x(z)$ and $B_y(z)$ data was filtered out in order to reveal the longer scale random perturbations using an integral of the field at each point along the z-axis taken from $z-\lambda_W/2$ to $z+\lambda_W/2$, where λ_W is the wiggler period, 44.44 mm (that is, a moving average, see Fig. 2).

It should be clarified, at this point, that the filtering of the wiggler-periodic field components in $B_y(z)$ and $B_x(z)$, which was needed in order to reveal the slowly varying random magnetic perturbation component, does not compromise the efficacy of the repair process. One should note that the wiggling amplitude due to the periodic wiggling field is inversely proportional to k_w^2 (Eq. (5)). Thus, the wiggling amplitude in the x-dimension (and certainly in the y dimension, if there is any) is smaller than the transverse excursion deviations due to the slowly varying random magnetic field perturbations.

The measurements off the central axis before disassembling the focusing magnets were used only to confirm the model of the magnetic fields expressed in Eqs. (1), (2), (8), and (9) and determining α_R. For constructing the 3D field of the wiggler we used only the measured data of $B_y(0,0,z)$ and $B_x(0,0,z)$ along the axis of the wiggler without the lateral magnets. This data was inserted into the General Particle Tracer (GPT) code [14] together with the independently measured data of the taken apart focussing magnets which were measured individually, and was used to extrapolate the 3D field in the wiggler, and calculate electron trajectories (explained below).

The strengths of individual lateral focusing magnets were measured using a jig, which held the magnets at the same distance from the probe as the magnets would be from the central axis of the wiggler. The magnets B_x and B_y components were measured and used in the pairing algorithm described below. The spare magnets and those 23 pairs of focusing magnets removed had about 20% variation in their range of remnant magnetic field. Their y magnetic field, measured with the jig at a distance corresponding to the relative position of the wiggler axis, was about 150 G on the average with maximal variation $\sim\pm 15$ G. The deviations in the B_x field of these magnets from the ideal zero ranged from 0.04 to 25 G, which could be used to add or subtract from the B_x field by rotating them 180° about the y-axis.

When making measurements of the wiggler the probe sat within a metal block, which was moved along the inside of the wiggler. The outer dimensions of the block were slightly smaller than that of the wiggler in order to allow it to pass through, whilst the probe was positioned at the centre of the block. To compensate for the uncertainty of the position of the block within the wiggler and that of the position of the hole at the centre of the block, each field was measured four ways, with the block and wiggler in different vertical orientations about the z-axis. These measurements were averaged to determine the field along the central axis.

2.1. Optimizing the wiggler beam-acceptance

Before attempting to compensate for the field imperfections, the first task was to optimize the beam focussing magnet configuration, in order to increase the beam phase-space acceptance of the wiggler, that is, to reconfigure the spacing and average strength of the focusing magnets in order to maximize the range of input trajectories (angle as well as initial x–y displacement from the central axis) of electrons, which can successfully traverse the wiggler.

The average field gradient of the wiggler that was measured before the repair was found to be $\alpha_R=32$ G/mm. Requiring equal focussing in the vertical and lateral dimensions implies $k_{\beta x}$ should approximately equal $k_{\beta y}$. This corresponds according to Eqs. (14)–(16) to a quad field gradient of $\alpha_R=14$ G/mm. To attain the reduced value of α_R we resolved to extend the spacing between the focussing magnets and so use fewer. It was calculated that 17 equally–spaced magnets of an available set would produce an integrated average strength closer to the optimal value but not leave too large gaps in the focussing field. So the effective α_R was altered to 20 G/mm.

The beam phase-space acceptance of the wiggler is determined by the maximum excursion off axis $\bar{x}_{max}$, $\bar{y}_{max}$ due to betatron oscillation that one permits in order to avoid hitting the transport walls along the wiggler:

$$|\bar{x}(z)| < \bar{x}_{max} \tag{19}$$

$$|\bar{y}(z)| < \bar{y}_{max} \tag{20}$$

where $\bar{x}(z)$ and $\bar{y}(z)$ are given by Eqs. (11)–(13).

Since at low acceleration energies (as in the present case) there is more than a quarter betatron oscillation period along the wiggler ($k_\beta L_W > \pi/2$), it is not enough to satisfy $|\bar{x}_0| < \bar{x}_{max}$, $|\bar{y}_0| < \bar{y}_{max}$ at the entrance to the wiggler, and inequalities (19) and (20), must be satisfied along the entire wiggler length, which sets limits also on the electron entrance angles $x_0' = \upsilon_{x0}/\upsilon_{z0}$, $y_0' = \upsilon_{y0}/\upsilon_{z0}$.

Figs. 3 and 4 show the elliptical phase-space acceptance boundaries (x_0, x_0') and (y_0, y_0') before and after the reconfiguration of the focussing magnets. Each data point (x_0, x_0') and (y_0, y_0') corresponds to an extreme trajectory that reaches correspondingly

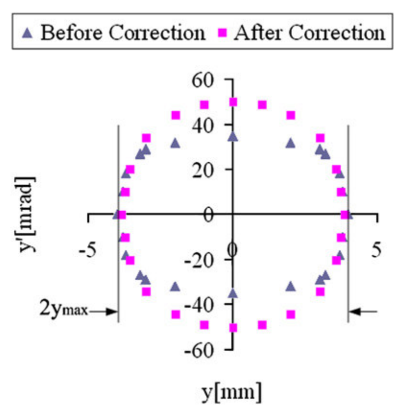

Fig. 3. Phase-space acceptance as a function of displacement (x-axis) and angle (y-axis) in the y–z plane.

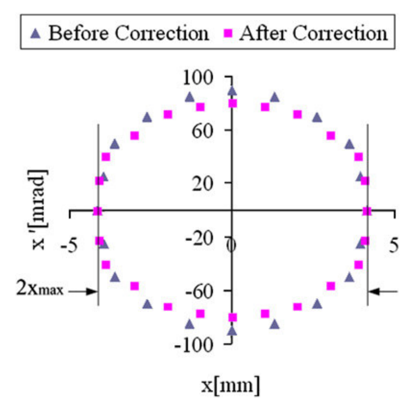

Fig. 4. Phase-space acceptance as a function of displacement (x-axis) and angle (y-axis) in the x–z plane.

the value $\bar{x}_{max}$ or $\bar{y}_{max}$ during transport along the wiggler. This was verified by employing 3D GPT simulations of the extreme particle trajectories.

Any electron within the phase-space acceptance ellipses of Figs. 3 and 4 will successfully traverse the resonator without striking the walls. The principal result of the change is the angular acceptance, going from $-90 < x' < 90$ mrad and $-35 < y' < 35$ mrad before repair, to $-80 < x' < 80$ mrad and $-50 < y' < 50$ mrad after the repair. Assuming the electron beam is roughly symmetric in the x–z and y–z planes, the increase in the y' acceptance at the price of a small reduction in x' acceptance is beneficial. We can conclude that the wiggler beam-acceptance is improved.

2.2. Synthesis of the 3D virtual magnetic field

A great advantage of the repair procedure proposed here is the model that enables us to synthesize the 3-D magnetic field for any permutation of sorted focusing bar magnets based on their individual measurements and the wiggler field measured on axis and analytically extended off axis. Having this virtually synthesized 3-D field makes it possible to calculate with GPT the expected electron beam trajectories for the given choice of bar magnets permutation and assess the improvement. Our model for the 3D magnetic field of the wiggler is based on the experimental verification that the geometrical periodicity of the wiggler construction is accurate, and that the perturbations to the magnetic fields are due to variations in the magnitude and orientation of the magnetization of the bar magnets or possible inhomogeneity and permeability differences in the blocks of the wiggler and focussing magnets. The variations of these field perturbations as a function of (x,y) are small in proximity to the axis. Consequently, we assumed that the x component of the real wiggler field $B_x^W(x,y,z)$ is approximately equal to the filtered x component of the field measured on axis $\overline{B}_x^{meas}(x=0,y=0,z)$ And the y component of the wiggler is the unfiltered $B_y^{meas}(x=0,y=0,z)$ measured on axis multiplied by $\cosh(k_W y)$ (as in Eq. (1)). So the 3D real wiggler magnetic field (without the focussing magnets) is modelled by

$$B_x^W(x,y,z) = \overline{B}_x^{meas}(x=0,y=0,z) \tag{21}$$

$$B_y^W(x,y,z) = B_y^{meas}(x=0,y=0,z)\cosh(k_w y) \tag{22}$$

To complete the principal model and enable 3D trajectory simulations, also the map of B_z was required. This magnetic field component distribution is dependent on the other components through Maxwell equations. Using $\vec{\nabla}\cdot\vec{B}=0$ and assuming that the field perturbation B_x is nearly uniform as a function of x and y near the axis (see Eq. (21)), the $B_z^W(x,y,z)$ field was calculated from the interpolated (using a cubic spline) measured B_y data using a simple finite difference method:

$$B_z^W(x,y,z) = \frac{1}{k_w}\frac{d\overline{B}_y^{meas}}{dz}(x=0,y=0,z)\sinh(k_w y) \tag{23}$$

Finally the fields of the individual focussing magnets were programmed into GPT and so were superimposed on the 3D wiggler field. The number of focussing magnets in the GPT simulation code was set in accordance with the conclusion of the previous sections. Namely, only 17 pairs of 50.8 mm long magnets were used, spaced equally along the wiggler length with 21 mm thick Teflon spacers.

2.3. Focusing magnet sorting algorithm for compensating wiggler magnet imperfections

In order to deal with the background random perturbation fields, the filtered data of the fields along the length of the wiggler was divided into 17 sections of length 71.8 mm, corresponding to the period of the proposed introduction of 17 focussing magnets. The average background wiggler imperfection field in each of the 17 regions was determined by integration of the interpolated filtered data. This approach of averaging the field in the sections was thought to be reasonable as the random perturbation field changes slowly with distance over each of the sections. This was not done for the data in the first and last regions at the start and end of the wiggler as the fields there were not sinusoidal. These regions were treated separately. The principle of the imperfection correction scheme was to annul these average field deviations in the 17 sections by proper choice of their corresponding focussing magnet pairs.

The results of the averaging for each region were stored in separate 1D matrices, one for B_x and one for B_y. From a list of all the available magnets, the lateral focussing magnets in use and other spare magnets, two 1D matrices of their measured B_y and B_x values were formed. These B_y and B_x values were the maximum field values measured with the jig at a position corresponding to the position of the assembled magnet bars relative to the wiggler axis. The field on axis of each magnet bar actually protruded beyond the length of the section that it needed to repair; however its integrated value was approximately equal to that of a uniform magnetic field along the same section, and therefore its integrated angular deflection effect is approximately equal to what is needed for cancelling the deflection effect of the average field perturbation in this section.

The procedure used for choosing the best pair of magnets required that their combination would minimize the perturbation field within a particular region. The first step was to find the pairs that minimized the B_x field, then the pairs that minimized B_y, and finally, which combinations would minimize the perturbations to both axes.

A square matrix was formed of the sums and differences of the B_x fields of the magnets:

$$B_{xm,n} = (1-\delta_{mn})\big|\,|B_{xv}| + \mathrm{sgn}(m-n)|B_{xm}|\,\big| \tag{24}$$

This matrix describes all the possible arrangements of B_x. The matrix for the B_y values was simpler:

$$B_{ym,n} = |By_n - By_m| \tag{25}$$

This was because the orientations in which the B_y field could be placed were limited by the wiggler setup, which called for the lateral focussing magnets on the left side to be pointing in the $+Y$ direction and the magnets on the right side to be pointing in the $-Y$ direction such that the B_y field on axis cancelled.

As there were 66 available focusing magnets (46 disassembled from the wiggler and an additional 20 spare magnets), two 66×66 matrices were formed from Eqs. (24) and (25). The pairing for the 1st and 17th position was left till the end. Each of the pairs for the intervening sections was chosen using the following procedure.

The averaged B_x and B_y backgrounds of each of the sections were subtracted from each of the matrix elements of Eqs. (24) and (25), respectively, resulting in two new 66×66 matrices for each of the 17 sections. The minimum value in each matrix represented the best combination for either the B_x or B_y axis. Equal weight was given to the importance of minimizing the perturbations to the B_x and B_y fields.

The two new matrices for each section were then added and the location of the minimum value of the resultant matrix for each section informed us on which pair of magnets minimizes the perturbations (in that region). The mth and nth row of the matrix represented the mth and nth values of a 66×1 matrix that was the list of the available magnets. The field at the entrance and exit to the wiggler, the 1st and 17th position, were not amenable to the same treatment. Whilst it was desirable to minimize B_x at the entrance, at the end it was desirable to use small B_x and B_y components to correct any angular deviation of the beam leaving the wiggler as was determined by GPT trajectory simulation. The B_y components at the entrance had to be chosen such that the electron was deflected into the correct undulating trajectory. The output of the sorting algorithm was a list of 17 magnet pairs listed in their optimal position order along the wiggler.

After deciding on an optimal reconfiguration of the focusing magnets based on the magnet sorting algorithm described above, we constructed in GPT the virtual 3-D synthesized field of the wiggler and the focusing magnets intended to be assembled.

The 3D field distribution of a rectangular magnet bar is calculated in GPT on the basis of a surface "magnetic charge" model (similar to [13]) based on the data of the average remnant magnetization of the individual focusing magnet bars in both transverse (x and y) dimensions, which were measured as described before with a special jig. The wiggler field 2D field distribution (y, z) was synthesized from the on axis field measurement using Eqs. (22, 23) (x variation of the field was neglected in the range of the beam's traversal). A special routine was provided by Pulsar Physics for implementing this algorithm in GPT. The synthesized 3D magnetic field composed of the modelled wiggler field and focussing magnet fields, was used in GPT for simulating the expected e-beam trajectories after reassembly of the focusing magnets and the output served to assess the quality of the intended repair.

In order to evaluate the repair of the wiggler after assembly, the B_x and B_y fields on axis were re-measured after the lateral focussing magnets had been re-arranged according to the results of the algorithm. The field measured on axis after the repair included the field of the lateral magnets. To avoid duplicating the field of the lateral magnets using GPT, the field of the lateral magnets on axis was deducted from the measured data on axis and this was used for $B_x^{meas}(0,0,z)$ and $B_y^{meas}(0,0,z)$ in Eqs. (21)–(23) for modelling the 3D field of the wiggler alone. The simulated 3D field of the lateral bar magnets could then be programmed in (as each of the individual lateral magnets had been measured separately).

3. Results

Figs. 5 and 6 display the magnetic field on axis with the focusing magnets assembled before and after repair, with the wiggling periodicity filtered out. Inspection of Figs. 5 and 6 seems to show significant improvement in $\overline{B}_x(z)$ and a small improvement in $\overline{B}_y(z)$. However, as indicated before, the wiggler field deviation data is not the most important criterion for the quality of the repair; rather it is the actual trajectories, simulated using the full 3D field that was synthesized from the measured fields.

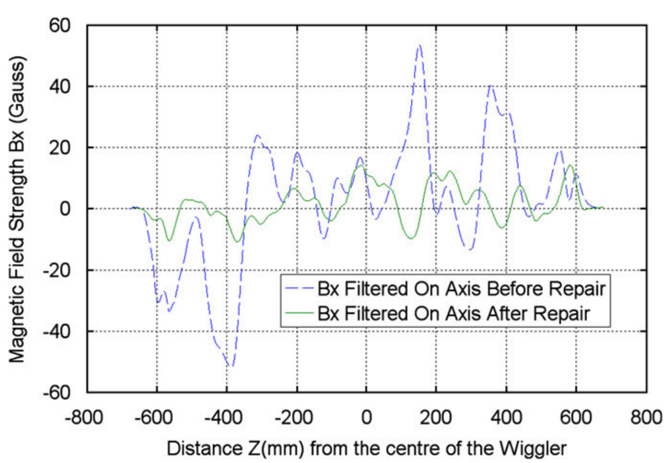

Fig. 5. Filtered B_x perturbation measured along the central axis before and after optimization.

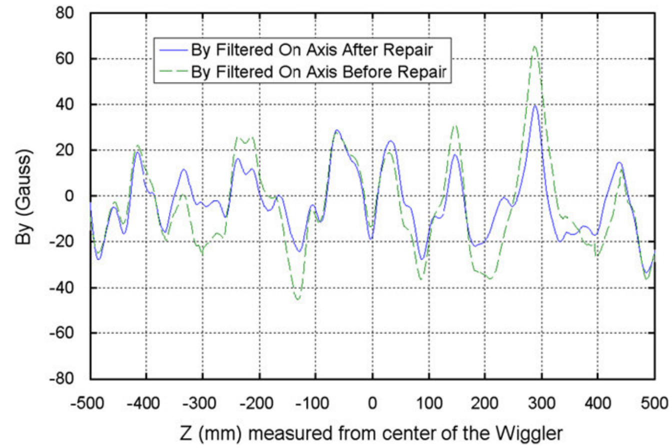

Fig. 6. Filtered B_y perturbation measured along the central axis before and after optimization.

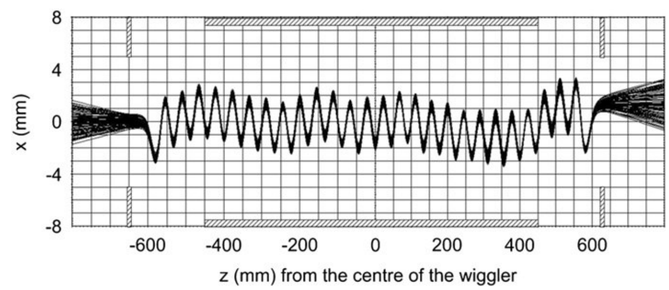

Fig. 7. Trajectories in the x–z plane of an electron beam passing through the wiggler.

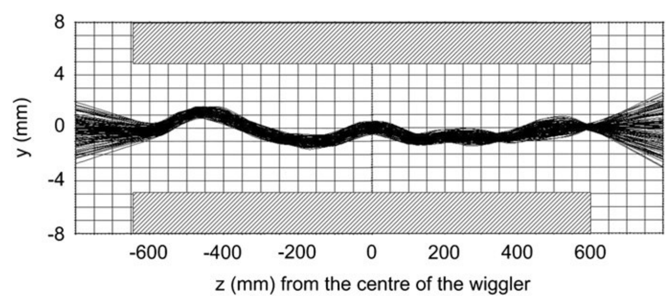

Fig. 8. Trajectories in the y–is plane of an electron beam passing through the wiggler.

Figs. 7 and 8 show the GPT simulation results of the electron beam propagation through the wiggler using the fields measured after the optimization of the magnets. The normalized emittance value for these graphs is 6.5π.

The electron beam parameters we see in Figs. 7 and 8, such as the wiggling amplitude and beam diameter, are similar to that simulated for an ideal wiggler without any perturbations to the field. The beam shown in Figs. 7 and 8 consists of 25 sample trajectories representing a finite emittance beam of total current 1.75 A. The positions of the walls of the resonator waveguide are indicated on the top and bottom of Figs. 7 and 8, positioned at ± 7.5 mm in the y–z plane and ± 5.35 mm in x–z plane. The simulations were run assuming a large emittance beam, indicating that good beam transport is possible through the aperture of the waveguide.

4. Conclusion

We have demonstrated that it is possible to ameliorate the effect of field imperfection caused by variations in field strength and polarization orientation of the main wiggler magnets by selecting appropriate magnets for the guiding quadrupole field and pairing them optimally. The selection is achieved using an algorithm that is not computationally demanding. It was possible to employ the matching algorithm based on a single Hall probe measurement along the wiggler axis, measurement of the individual bar magnets, and a 3-D field model that we developed for computing the combined 3D field of the wiggler and the focussing bar magnets. This virtual field mapping makes it possible to simulate the electron trajectories in the repaired wiggler, and evaluate the wiggler field and beam transport characteristics before placing the wiggler in the accelerator. We suggest this method as a simple scheme for improving the transport parameters of imperfect permanent magnet linear wigglers.

Acknowledgement

We thank S.B. van der Geer and M.J. de Loos of Pulsar Physics for programming assistance with GPT. We thank Joachim Pflueger of DESY, Hamburg, for his advice. This research was supported in part by the Israeli Science Foundation, Grant no. 353/09.

References

[1] A. Gover, Laser: free electron lasers, Encyclopedia of Modern Optics, Elsevier, 2005.
[2] K. Halbach, Nuclear Instruments and Methods 169 (1980) 1.
[3] H.S. Marks, M. Volshonok, E. Dyunin, A. Gover, Y. Lasser, R. Shershevski, A. Yahalom, Improvement of a wiggler by single axis measurement, virtual synthesis, and relocation of magnets, in: Proceeding of FEL 2009, Liverpool, UK, 〈http://accelconf.web.cern.ch/AccelConf/FEL2009/papers/wepc08.pdf〉.
[4] J.N. Ortega, C. Bazin, D.A.G. Deacon, Journal of Applied Physics 54 (9) (1983) 4776.
[5] R.A. Cover, B.L. Bobbs, G. Rakowsky, M.M. Johnson, S.P. Mills, Nuclear Instruments and Methods in Physics Research A296 (1990) 603.
[6] B. Diviacco, R.P. Walker, Nuclear Instruments and Methods in Physics Research A 368 (1996) 522.
[7] R. Hajima, F. Matsuura, Nuclear Instruments and Methods in Physics Research A 375 (1996).
[8] B.J.A. Shepherd J.A. Clarke, Construction and Testing of a Pair of Focussing Undulators for Alpha-X, in: Proceedings of EPAC 2006, pages 3580–3582.
[9] S.C. Gottschalk, D.C. Quimby, K.E. Robinson, J.M. Slater, Nuclear Instruments and Methods in Physics Research A 296 (1990) 579.
[10] R.W. Warren, C.J. Elliott, New system for wiggler fabrication and testing, in: Proceedings of the Adriatico Research Conference on Undulator Magnets for Synchrotron Radiation and Free Electron Lasers, Trieste, 23-26 June 1987.
[11] A. Gover, H. Freund, V.H. Granatstein, J.H. Mc Adoo, Chai-Mei Tang, Infrared and millimeter wave, in: Ed.,in: K. Button (Ed.), Design Considerations for Free Electron Lasers Driven by Electron Beams from RF Accelerators, Vol. II, Academic Press, 1984 (Chapter 8).
[12] M. Cohen, An Analysis of a Prebunched Beam Free-Electron laser, Ph.D. Thesis, Tel Aviv University, 1995.
[13] L. Elias, R.C.J. Hu, G. Ramian, Properties of the USCB FEL wiggler, Proceedings of the International FEL Conference, SPIE vol. 453, 1983 p. 160.
[14] 〈http://www.pulsar.nl/gpt〉 (last used 20/08/11).
[15] A. Gover, P. Sprangle, Journal of Applied Physics 52 (1981).